

Article

The Investigation of Stefan Luchian Heritage Paintings—A Multi-Analytical Approach

Andrei Victor Oancea ¹, Bogdana Simionescu ², Laura Elena Ursu ¹ , Mioara Murariu ¹, Marius Dobromir ³, Maria Geba ^{2,†}, Lacramioara Stratulat ² and Mihaela Olaru ^{1,*}

¹ “Petru Poni” Institute of Macromolecular Chemistry, 41A Gr. Ghica Voda Alley, 700487 Iasi, Romania; oancea.victor@icmpp.ro (A.V.O.); ursu.laura@icmpp.ro (L.E.U.); mioara.murariu@icmpp.ro (M.M.)

² “Moldova” National Museum Complex, 1 Stefan cel Mare si Sfânt Square, 700028 Iasi, Romania; simionescubogdana@yahoo.com (B.S.); stratulatlacramioara@yahoo.com (L.S.)

³ Research Centre on Advanced Materials and Technologies, Department of Exact and Natural Sciences, Institute of Interdisciplinary Research, Alexandru Ioan Cuza University of Iasi, 11 Carol I Blvd., 700506 Iasi, Romania; marius.dobromir@uaic.ro

* Correspondence: olaruma@icmpp.ro; Tel.: +40-760289368

† Deceased.

Abstract: Based on a multi-analytical approach involving mobile techniques and lab-based devices (XPS, portable and micro-Raman spectroscopies, and ATR-FTIR spectroscopy, combined with SEM/EDS and optical microscopy), this study presents the first in-depth investigation of two cultural heritage artworks painted by the famous Romanian artist Ștefan Luchian. The research highlights the artist’s use of a wide range of colors, with his palette including classic pigments such as ochers, lead white, barium white, zinc white, and viridian, as well as contemporary colors such as cobalt purple, alizarin crimson, and the little-known indium yellow. Additionally, attempts are made to characterize the binders used in the paintings, which include linseed oil and animal glue. Beyond identifying the types of pigments and materials used by the artist and assessing the degradation stage of the paintings, this study is the first to provide information regarding the use of In₂O₃ as a yellow pigment in artwork.

Keywords: Luchian; pigments; spectroscopy; In₂O₃; degradation phenomena



Academic Editor: Ioannis Karapanagiotis

Received: 20 November 2024

Revised: 26 December 2024

Accepted: 8 January 2025

Published: 13 January 2025

Citation: Oancea, A.V.; Simionescu, B.; Ursu, L.E.; Murariu, M.; Dobromir, M.; Geba, M.; Stratulat, L.; Olaru, M. The Investigation of Stefan Luchian Heritage Paintings—A Multi-Analytical Approach. *Heritage* 2025, 8, 26. <https://doi.org/10.3390/heritage8010026>

Copyright: © 2025 by the authors. Licensee MDPI, Basel, Switzerland. This article is an open access article distributed under the terms and conditions of the Creative Commons Attribution (CC BY) license (<https://creativecommons.org/licenses/by/4.0/>).

1. Introduction

The identification of the pigments and materials used by the artist in a painting is a mandatory step to be considered before any conservation procedure is taken into account. To conserve and restore works of art, it is vital to identify both the materials employed by the artist and the degradation processes affecting the painting. Canvases may be regarded as complex heterogeneous structures in which multiple interactions between various constituents, in addition to aging and degradation phenomena, take place. In order to understand the intrinsically complex nature of these phenomena, detailed and advanced analytical techniques are necessary to obtain information on the nature of the materials used by the painter and of the ongoing processes of degradation.

A disciple of Nicolae Grigorescu, Ștefan Luchian (1868–1916), consecrated as a “flower painter”, is one of the most representative modern post-impressionist Romanian painters, who established a scientific basis in modernist pictorial art, both visually and conceptually [1]. Ștefan Luchian is known to be the first Romanian painter who, in order to underline Romanian art’s distinct personality within the European context, was inspired by

traditional mural paintings of medieval churches and by Romanian traditional art, simplifying and underlying some elements and overshadowing others. A colorist by excellence, Luchian expressed his lyrical spirit by converting nature into linear syntheses and bright chromatic harmonies. To obtain his desired hues, Luchian used direct mixing of several pigments in his easel painting, a technique previously adopted by Grigorescu. Regarding the painting of flowers, Luchian's technique implied the superposition of a dense paste in successive layers, by using a knife or by modeling it with a brush, in a stormy texture replete with nuances and reflexes, thus conferring an irregular topography to corollas [2].

Although the innovative contribution brought to the Romanian painting by the famous painter Ștefan Luchian comprises more than 100 works, there is no comprehensive study regarding the identification and structural characterization of materials and pigments used by this artist, as well as of the degradation processes affecting his work. The present study is a multi-analytical investigation focused on the structural characterization of the materials and pigments used by Ștefan Luchian in two heritage artworks, i.e., *Chrysanthemums* and *Roses*, belonging to the "Moldova" National Museum Complex. A previous investigation conducted on the same artworks was limited to a rather brief analysis by means of portable XRF and Raman spectrophotometers [3]. The presence and identification of In_2O_3 through analysis of some microscopic fragments of paint layers through SEM/EDS and XPS measurements was thoroughly studied. Although indium yellow, the generic name for either indium oxide (In_2O_3) or sulfide (In_2S_3), has been mentioned since 1869 for its possible use as a pigment [4], only one reference regarding the use of In_2O_3 as a precursor for the obtaining of YInMn blue pigment (YInMn stands for the component elements, i.e., yttrium, indium, and manganese) has been published in the literature [5]. To our knowledge, no reports on the use of In_2O_3 as a yellow pigment in an artwork have been previously published.

2. Materials and Methods

The study of the artwork included on-site investigations with portable equipment, and an in-depth analysis of microscopic fragments using tabletop instruments. Raman measurements, performed directly on the paintings, were recorded using a portable Raman spectrophotometer (R-3000CN from Raman Systems, Woburn, MA, USA) with a 785 nm diode laser, with a spectral resolution of 2 cm^{-1} and integration time of 10 s. The selected laser power for these analyses varied in the range of 10–50 mW, depending on the specimen. In the used configuration, the laser spot was about 0.1 mm in diameter, allowing a real spatial resolution in the range of few millimeters to be obtained. Due to the relatively large spot size, the laser power per area was weak in order to avoid any damage to the paintings. The spectrometer was calibrated before each experimental session using the Raman peak of a silicon crystal at 520.5 cm^{-1} .

Analyses using invasive techniques were performed on microscopic samples collected from under the picture frames to ensure no damage to the painting's surface. These included small grains, generally less than $1 \times 1\text{ mm}$ in size, collected from stains of different colors, as well as a small canvas fragments from the back of the *Chrysanthemums* painting that contained small smudges approx. $2 \times 2\text{ mm}$ in size. The samples were named as follows: microscopic grains from *Roses*—LIB (point of collection 1', Figure 1a), microscopic green grains from *Roses*—LIB_V (point of collection 2', Figure 1a), microscopic grains from *Chrysanthemums*—LIIB (point of collection 1', Figure 1b) and *Chrysanthemums*—LIIB_V (point of collection 2', Figure 1b), and a canvas fragment with blackish paint smudges from *Chrysanthemums*—LIIA (point of collection 3', Figure 1b). For the analyzed samples, the surface elemental composition of the samples and the chemical states of oxygen (O), carbon (C), sulfur (S), calcium (Ca), lead (Pb), and silicon (Si) were derived from X-ray Photoelectron Spectroscopy (XPS) measurements. These were performed with a PHI 5000

VersaProbe, ULVAC-PHI (Chikasaki, Japan) spectrometer, equipped with a monochromated AlK α X-ray source ($h\nu = 1486.6$ eV) under a take-off angle of the photoelectrons of 45° . The measurements were recorded using the following settings: pass energy = 58.7 eV, energy step = 0.1 eV, time/step = 20 ms, X-ray beam energy = 25 W, and X-ray beam diameter = 100 μm . Following a standard procedure [6], the high-resolution XPS spectra of O 1s, C 1s, S 2p, Ca 2p, Pb 4f, Si 2p, Zn 2p, Co 2p, Ba 3d, and In 3d were used in the identification of compounds. Due to the small size of the microscopic green grains from both paintings (samples LIB_V and LIIB_V), spectra could not be recorded for these. For the larger LIIA sample, four spectra were collected: one in the region of the canvas, two in the overall area of the blackish paint smudges, and a final one in an area of interest that contained grains of indium yellow. The calibration of the binding energy (BE) scale was performed by considering the BE of the C 1s peak (284.8 eV). Peak deconvolution was performed using the CasaXPS 2323PR1-0 software. ATR-FTIR spectra were produced with a Bruker Vertex 70 instrument (Billerica, MA, USA), in the 4000–6000 cm^{-1} region, with a resolution of 2 cm^{-1} , by performing 64 scans at room temperature, using the ATR technique and the Opus 5 FTIR Software. ATR-FTIR spectra were recorded for all the samples, and for the larger LIIA sample, three spectra were recorded: one in the area of the blackish smudges and two in the area of the canvas without paint. For the microscopic samples extracted from the painting rims, the Raman spectra were recorded using a Renishaw InVia Reflex spectrometer with a 632.8 nm He-Ne laser (maximum laser power 50 mW). All the spectra were collected through a 50 \times objective, giving a footprint of about 1 μm . The laser power density on the samples was minimized to 5 mW to avoid any thermal damage. Each spectrum was recorded using a 1 s accumulation time for 15 spectral accumulations to achieve an acceptable signal-to-noise ratio. The resolution of the recorded spectra was 2 cm^{-1} . All the samples taken for analysis were examined in several regions in order to identify as many pigments as possible. The spectrometer was calibrated before each experimental session using the Raman peak of a silicon crystal at 520.5 cm^{-1} . The SEM images were obtained using a Quanta 200 scanning probe microscope, from FEI Company, Hillsboro, OR, USA with the following settings: 60 Pa void, 10 mm working distance, and an accelerating current of 20 KeV. Due to the small size of most of the microscopic fragments, and the desire to not contaminate them with material from the double-sided tape required for mounting them on Al conducting supports (and thus impede subsequent analyses), it was decided that only the canvas sample LIIA would be investigated by SEM/EDS. The sample was mounted on cylindrical-shaped Al conducting supports in order to perform the investigations. A Leica DM2500 M microscope (Wetzlar, Germany) with transmitted and incident light and fluorescence, and LAS Interactive Measurement software (<https://www.leica-microsystems.com/products/microscope-software/p/leica-las-x-ls/>) for image acquisition, were used to analyze the microscopic fragments. Graph creation for the FTIR, Raman, and μ -Raman spectra, and background subtraction for the cobalt purple spectrum, was performed using Origin software (<https://www.originlab.com/>).

The techniques used in this study (optical microscopy, SEM/EDS, XPS, Raman spectroscopy, μ -Raman spectroscopy, and FTIR spectroscopy) have been widely used in the study of cultural heritage objects, as the following reviews describe in detail [7,8].



Figure 1. Investigated canvases: (a) *Roses*: 1, 4, 5, 6, 7, 8, 11, 12, 13, 14, and 18—analysis points where portable Raman spectra with identifiable bands were recorded, and 1', 2'—overall area from which samples were collected beneath the frame; (b) *Chrysanthemums*: 8, 9, 11, 12, 13, 14, 16—analysis points where portable Raman spectra with identifiable bands were recorded, and 1', 2', 3'—overall area from which samples were collected beneath the frame.

3. Results and Discussion

The two canvases, i.e., *Chrysanthemums* and *Roses* (Figure 1), belong to the painter's second artistic phase, characterized by the flowers theme (1907–1910), by significant brilliance, and by the study of chromatic forces. These heritage paintings were analyzed using XPS, portable and micro-Raman spectroscopy, and FTIR spectroscopy, as well as SEM/EDS and optical microscopies. Table 1 contains a list of all the identified pigments in the analyzed cultural heritage canvases.

Table 1. List of pigments identified through spectroscopic techniques, or whose use was established due to the presence of known common degradation products. Pigments were identified and characterized using the following techniques: a—XPS; b—SEM/EDX spectroscopy; c— μ Raman spectroscopy; d—portable Raman spectroscopy; and e—FTIR spectroscopy; and they were inspected with f—optical microscopy.

		Artwork						
		<i>Roses</i>			<i>Chrysanthemums</i>			
Color	Pigments/paint components	Painting	Samples		Painting	Samples		
			LIB	LIB_V		LIIA	LIIB	LIIB_V
White	Lead white		a, e	e	d, pts. 8, 11, 12, 18	b, e	a	
	Zinc white	d, pt. 6				a, b	a	
	Barium white	d, pts. 3, 7, 8, 11, 13	e	e		a, b, c	c	
	Calcium carbonate Gypsum		a, e	e		a, b, e b	a	
Black	Carbon black				c			
Blue	Prussian blue					b		
	Ultramarine					c		
	Azurite					c		
Green	Viridian					b, f		
	Cobalt green/Rinmann's green Copper-based green pigment					a, b		

Table 1. Cont.

		Artwork			
		Roses		Chrysanthemums	
Yellow	Indium yellow				a, b, f
	Strontium yellow			d, pts. 13, 14	b, e
	Cadmium yellow				b
	Yellow ochre				b
	Massicot				a, b, c
Red	Red ochre				b, c
	Vermillion	d, pts. 1, 4, 5, 6, 12, 15	c	c	b, c
	Alizarin crimson PR 83	d, pt. 14		d, pt. 9	
	Phenylazonaphthol PR 57:1				c
Brown	Cassiterite				c
	Burnt umber/Sienna				b
Purple	Cobalt violet		e	e	b, c

3.1. SEM/EDS Microscopy

Generally, the most abundant elements found in the EDS analysis of LIIA were C and O, in concentrations usually exceeding 20%, which is consistent with the extensive use of a binder in the painting layer. With the exception of zinc and chrome (generally having values up to 2–3%), in the areas with a high binder content, the concentrations of other elements were usually below 1%. However, for certain grains, the EDX measurements showed high readings for the pigment constituents. The EDS investigations in which the atomic concentration of various grains are mentioned are illustrated in Table S1 (ESI). The presence of Ba, Zn, and Ca in multiple analysis points indicates the combined use of barium white (BaSO_4), zinc white (ZnO), and calcium carbonate (CaCO_3) to obtain the white color. Although the overall amount of these elements slightly varied, the analysis showed the presence of several grains where the pigments appeared individually. As such, barium white was revealed by larger grains containing Ba (5.3%) and S (5.4%) in much higher amounts as opposed to all other elements, except for C and O. One grain with a Ca concentration of 14.9% showed the use of calcium carbonate, while another one, where the Ca concentration reached 8.9% and the Zn concentration reached 6.7%, also emphasized the use of both calcium carbonate and zinc white. An area rich in Ca (5.2%) and S (4.7%) revealed the use of plaster containing gypsum (CaSO_4) in the preparation layer. However, the presence of Pb, most likely in the form of lead white pigment ($\text{PbO}/2\text{PbCO}_3 \cdot \text{Pb}(\text{OH})_2$), used either as a whitener or as a siccative agent, was confirmed by SEM/EDS investigation in many analysis points. The overall low concentration in which Pb was found indicated that the painter made little use of this pigment, and preferred other shades of white.

Many of the analyzed points contained significant amounts of Sr, with values reaching up to 2.3% in the investigated areas. A closer look at the atomic concentrations of the other elements in the investigated points revealed that Sr was present in high amounts (more than 1%), as well as Cr. This type of elemental composition matches the structure of strontium yellow (SrCrO_4) pigment.

The identification of high amounts of Fe (15.3%) and Cr (12.10%), while other metals were present below 1.2% in an investigated area, is consistent with the use of either siderin yellow ($\text{Fe}_2(\text{CrO}_4)_3$) or a combination of pigments containing Fe, i.e., red ochre (containing hematite— Fe_2O_3) or yellow ochre (containing lepidocrocite— $\gamma\text{-FeO}(\text{OH})$ —with viridian (Cr_2O_3)). Aside from the iron compounds providing the color, ochres also

contain impurities in the form of aluminosilicates or quartz. At the analyzed point, Al and Si were found in a concentration of 1.1% and 1.7%, respectively. Therefore, the use of a mixture of pigments at the analyzed point is much more likely, as opposed to siderin yellow.

Another yellow pigment that was identified in the SEM/EDS analysis was cadmium yellow (CdS). While cadmium was present in many of the analysis points, the presence of this cadmium yellow pigment was highlighted by measurements performed in two distinct areas containing high amounts of cadmium (10.4% and 13.6%) and sulfur (9.5% and 13.3%). Moreover, in Figure S1, ESI shows the information regarding the optical microscopy, SEM image, and elemental composition of a yellow grain containing significant amounts of cadmium (3.1%) and sulfur (2.6%), pointing out the presence of cadmium yellow.

Regarding the blue pigments, two large grains were observed through optical microscopy and later identified using SEM/EDS analysis based on morphological landmarks (one of the grains is shown in Figure S2, ESI). The elemental composition of both grains showed high amounts of iron (5.3% and 10.1%), indicating that Luchian used Prussian blue ($\text{Fe}_4[\text{Fe}(\text{CN})_6]_3$) in his works of art. Besides the presence of a high amount of iron (5.3%), the largest grain showed a high concentration of Co (2.7%). The most common blue pigments containing Co are cobalt blue (CoAl_2O_4), cerulean blue ($\text{CoO} \cdot n\text{SnO}_2$), and enamel (an alkaline silica containing small amounts of Co). The analyzed blue pigment cannot be cobalt blue, due to the analyzed pigment containing a small concentration of aluminum (0.4%) vs. cobalt, or cerulean blue, because of the absence of tin. Also, no relation between the constituent elements of enamel pigment could be found in the SEM/EDS analysis, with its silicon (0.6%) and potassium (almost non-detectable) percentages being significantly lower compared to cobalt (2.7%). The blue color of the analyzed grain suggests the use of Prussian blue pigment in combination with small amounts of cobalt green, a blue-green pigment obtained by mixing cobalt oxide with either zinc or iron oxides [9].

Several of the purple grains that were observed using optical microscopy showed significant values for phosphorus (7.5%) and cobalt (1.3%) when their elemental concentrations were determined through SEM/EDS measurements (Figure S3, ESI). The presence of these elements is consistent with the use of a cobalt purple pigment, i.e., either cobalt phosphate $\text{Co}_3(\text{PO}_4)_2$ or its octahydrate form ($\text{Co}_3(\text{PO}_4)_2 \cdot 8\text{H}_2\text{O}$). An overall review of the analysis points where cobalt was present raises the possibility that another pigment may also be present. Aside from the purple grains in which it was identified, along with important quantities of phosphorus, cobalt also appeared in areas characterized by black, white and blue hues, as well as in the binder area. Even though no distinct green grains with a high concentration of only zinc and cobalt were identified, one cannot exclude the possibility that the artist also used Rinmann's green pigment ($\text{Co}_x\text{Zn}_{1-x}\text{O}$), a pigment with a similar structure to cobalt green, in which aluminum hydroxide is partially or totally replaced by zinc oxide [9]. The poor tinting strength of this pigment may explain why cobalt was found in a variety of analyzed points where the green color was not particularly obvious when using optical microscopy. At the same time, the low values of cobalt seem to also indicate that the artist made little use of Rinmann's green pigment, as is the case for lead white; this is another reason why large grains of this pigment were not observed.

SEM/EDS measurements performed on two red grains evidenced the presence of high amounts of Hg (12.4% and 6.4%) and S (11.6% and 6.4%), while other important elements had concentrations below 2%, which may be attributed to the presence of vermilion pigment (HgS). At the same time, the elemental concentration of many other analyzed points revealed noticeable quantities of mercury, indicating an extensive use of this brilliant red pigment.

Chrome appeared in many of the investigated points, indicating that Luchian had a preference for the color green, shown by his extensive use of the viridian pigment

($\text{CrO}_3 \cdot 2\text{H}_2\text{O}$) (Figure S4, ESI). The green grains identified by optical microscopy showed a particularly high concentration of chrome. While other authors indicate that viridian could also be formed during the reduction process of PbCrO_4 [10], this is not the case here, since, in several grains, the concentration of Cr was in such large amounts that it sometimes reached values up to 8%, while Pb did not appear at values higher than 1%.

While viridian is the green pigment that Luchian used in the largest amounts, SEM/EDS measurements performed on a large green grain observed with optical microscopy (Figure S5, ESI), showed high amounts of copper. The most common copper-based green pigments found in art works are malachite ($\text{Cu}_2\text{CO}_3(\text{OH})_2$), neutral and/or basic verdigris, and copper resinate. Unfortunately, a clear identification of the copper-based green pigment was not possible, as this analysis technique is not able to differentiate between the three compounds.

While brown pigments could not be easily identified under optical microscopy, an area that was analyzed through SEM/EDS measurements showed the presence of high quantities of manganese (10.5%). While manganese is one of the major components of the brown umber pigment, i.e., mixtures of natural manganese, iron oxides, and hydroxides, or a minor component of Sienna, i.e., an earth pigment containing iron and manganese oxides, the presence of manganese oxides as components of clays cannot be excluded.

Several bright areas observed through optical microscopy were later analyzed using SEM/EDS (Figure 2), and revealed the presence of indium. The possible use of indium yellow (In_2O_3) as a yellow pigment was mentioned at the time of the production of the masterpiece, being considered “chiefly interesting in an artistic sense on account of its bright yellow color” [4]. The quantity of indium ranged from 20.3% to 22.2%, indicating very clearly that it could not come from impurities, and leading to the conclusion that indium yellow was intentionally used by the artist for its coloring properties.

While indium was identified based on EDS measurements, its absence in the XRF analysis performed on the same two paintings [3] can be attributed to a series of factors. One of the major issues encountered in identifying indium is the very small difference between the X-ray lines of this metal and the ones belonging to potassium. Consequently, the most intense X-ray lines of indium, i.e., $L\alpha_1$ (3.28 eV) and $L\alpha_2$ (3.27 eV), are situated very close to the $K\alpha_1$ (3.31 eV) and $K\alpha_2$ (3.31 eV) X-ray lines of potassium, while the $L\beta_1$ X-ray line of indium (3.58 eV) is in the vicinity of $L\alpha$ X-ray line of potassium (3.48 eV). As such, unless the user specifically knows of or is looking for indium in the analyzed sample, they may simply disregard any automated identification of the metal and attribute the signal to potassium, which is a much more common element found in various minerals and compounds used for the production of paintings. At the same time, the peak envelope of the software was not a good match for the assignment of the X-ray lines to the signals from other elements, due to significant differences in intensities and energy, as can be seen in Figure 2. The position of the $L\alpha_1$ line of potassium is slightly shifted in comparison to the spectrum, while in the case of the $L\alpha_2$ line of potassium, both the intensity and position do not match the spectrum when scaled to the $L\alpha_1$ line. The attempt to assign the two next features to the Ca $K\alpha_1$ (3.691 eV), $K\alpha_2$ (3.688 eV), and $L\alpha_1$ (4.012 eV) lines, again, does not match the envelope of the spectrum, but an adequate fit is obtained for the $L\beta_2$ (3.713 eV) and $L\gamma_1$ (3.920 eV) lines of In. In the low-energy region of the spectrum, the signal after C cannot be assigned to the $K\alpha$ (0.392 eV) line of N, as it is too shifted, but it corresponds to the M (0.368) line of In. Two other features close to 2.9 eV and 3.1 eV can also clearly be attributed to the L1 and Ln lines of In. Other reasons why indium was not present in the XRF measurements may come from the fact that, while the grains of the pigment contained a high amount of indium, this metal was not found in the surrounding regions (as can be

seen in Figure 2), and it is quite possible that the area measured by XRF did not contain any indium.

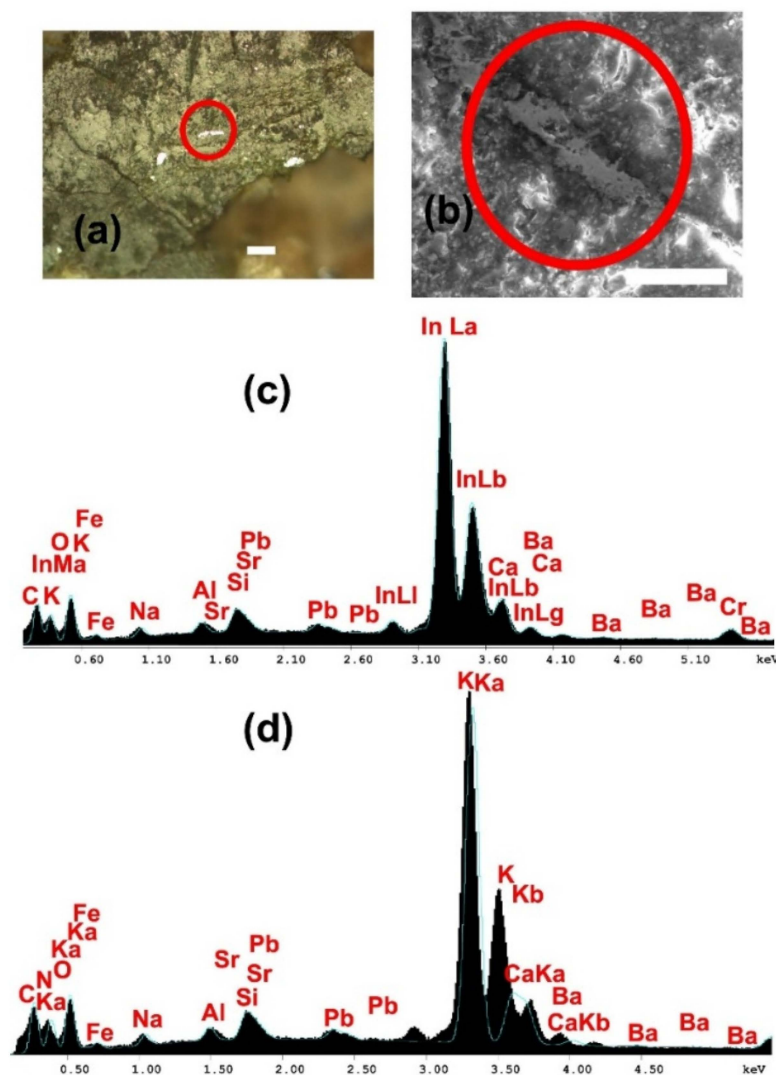


Figure 2. (a) Optical microscopy image of several In₂O₃ grains from *Chrysanthemums*, LIIA sample with an indication of the central grain shown in SEM, 0.1 mm scale, 10× objective; (b) SEM image of the central In₂O₃ grain, 30 μm scale; (c) EDS spectrum recorded for the central In₂O₃ grain, with indication of the position of element bands and In XRF characteristic band (In L_α, In L_β₁, In L_β₂, InL_γ and In M_α) fitting; (d) EDS spectrum recorded for the central In₂O₃ grain, with indication of the position of element bands and K and Ca characteristic XRF band (K K_α, K K_β, Ca K_α and Ca K_β fitting).

3.2. X-Ray Photoelectron Spectroscopy (XPS) Analysis

The assignment of XPS bands for LIB, LIB_V, LIIA analysis point 1, LIIA analysis point 2, LIIA canvas, and LIIA indium oxide grain samples can be found in Table S2 (ESI). XPS analysis of one yellow grain found on the canvas fragment belonging to *Chrysanthemums* revealed the presence of only indium, oxygen, and carbon elements (Figure 3). The C 1s spectrum evidenced carbon contamination during air exposure, with the XPS spectrum of the adventitious carbon consisting of hydrocarbon species of C-C/C-H type (284.83 eV), and carboxides containing C-O-C (between 286.1 eV) and O-C=O (288.91 eV) bonds, respectively [11]. The In 3d_{5/2} bands contain contributions from both In₂O₃ and In₀ with maximum intensities at 444.36 and 443.39 eV, while the binding energies of In 3d_{3/2} levels were found at 451.87 and 450.85 eV, respectively [12].

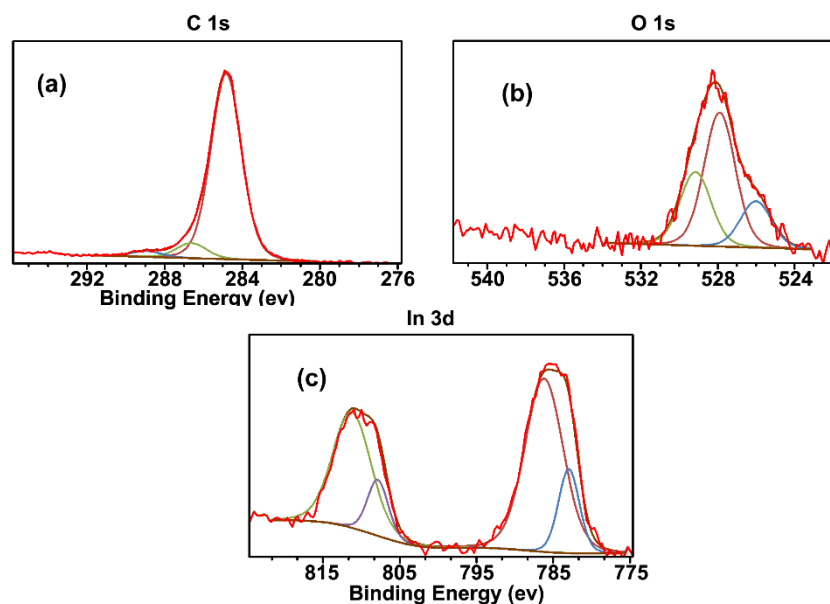


Figure 3. XPS spectra of (a) C 1s, (b) O 1s, and (c) In $3d_{3/2}$ and $3d_{5/2}$ peaks of In_2O_3 grain from sample LIIA, previously analyzed by SEM/EDS.

Regarding oxygen, the O 1s spectra showed the presence of three signals that can be attributed to In_2O_3 (530 eV) [13], to C-O-C (531.89 eV), and to the O-C=O (533.15 eV) groups from adventitious carbon [14]. The presence of only In, O, and C in the XPS spectra may indicate the use of $\text{In}(\text{OH})_3$ as a precursor for obtaining In_2O_3 through thermal decomposition. As follows, In_2O_3 forms upon ignition of $\text{In}(\text{OH})_3$ at 850 °C up to a constant weight, this process is followed by the heating of the resulting material for 30 min, in air, at around 1000 °C [15]. The appearance of metallic indium could be explained by the heating of In_2O_3 in an atmosphere of hydrogen [16] for at least 3 h. Under the action of visible light, In_2O_3 is known to exhibit a moderate photocatalytic activity for the production of hydrogen, i.e., 98.6 mmol of H_2 , after 3 h of light irradiation [17]. Most likely, indium yellow was chosen as a pigment due to its particular yellow color, containing shades of silvery white due to the presence of a small amount of metallic indium in its structure.

The presence of adventitious carbon was also evidenced in one analyzed sample from *Chrysanthemums* (Figure S6a, ESI). In the case of the other analyzed samples (Figures S7a, S8a, S9a and S10a, ESI), the C 1s spectrum displayed the presence of four signals attributed to the C-C/C-H (between 284.53 and 284.77 eV), C-O/C-OH/C-O-C (between 285.13 and 285.83 eV), C=O (between 287.06 and 287.3 eV), and O-C=O (between 288.56 and 288.82 eV) functional groups, these being characteristic of linseed oil or a binder [14]. For oxygen, the O 1s spectrum showed the presence of two signals that can be attributed to the C-O-C/O-C=O/C=O (between 531.66 and 532.32 eV) and O-C=O (between 533.15 and 533.77 eV) groups (Figures S6c, S7c, S8b, S9b, S10b, ESI) [12].

The identification of nitrogen in a sample from *Chrysanthemums* (Figure S7b, ESI) may suggest the presence of an animal glue, with bands characteristic of amide linkages appearing at 399.74 eV [18]. The other band, appearing at 405.63 eV, may be correlated with the adsorption of nitrate ions (NO_3^-) on the pigment layer's surface [19].

The appearance of Co $2p_{3/2}$ at 781.92 eV and of Co $2p_{1/2}$ at 797.23 eV, as well as of an O 1s peak at 531.66 eV (Figure S6b, ESI), may be related to the presence of a cobalt-doped zinc oxide structure with oxygen vacancies [20,21]. Taking into account the information from the SEM/EDS and optical microscopy investigations, and that the recipe for producing green cobalt-based pigments, such as cobalt green or Rinmann's green, involves the addition of small amounts of cobalt to ZnO, the presence of the cobalt-doped zinc oxide structure

seems to indicate the use of one of these two pigments. The attendance of Zn within the analyzed sample's wide spectrum (Figures S6d, S7d, S9c and S10g, ESI) may also be correlated with the usage of ZnO as a pigment, with the two strong peaks situated between 1022.4 and 1022.52 eV, and between 1045.25 and 1045.63 eV, being attributed to Zn 2p_{3/2} and Zn 2p_{1/2}, respectively [22] (p. 89). The O 1s peaks corresponding to oxygen bound to zinc were observed between 531.89 and 532.2 eV [23]. The presence of silicon within one sample (Figure S8d, ESI) may be associated with the presence of quartz-based impurities, with O1s, Si 2p_{1/2} and Si 2p_{3/2} peaks being observed at 532.33, 102.24, and 102.84 eV, respectively [13].

Alongside with linseed oil, the presence of carbonate species in the C1s region (290 eV, 290.4 eV) was also evidenced (Figures S7a and S8a, ESI). These species can be attributed to CO₃²⁻ ions from CaCO₃ [22] (p. 63) and PbCO₃ [24]. Additional peaks related to the presence of CaCO₃ could be found between 533.67 and 533.77 eV (O 1s of the oxygen atoms in carbonate ions), while the Ca 2p_{3/2} and Ca 2p_{1/2} peaks were located between 347.79 eV and 351.34 eV, respectively [25] (Figure S9d, ESI). Another point of analysis evidenced the occurrence of gypsum (CaSO₄·2H₂O) (Figure S10c, ESI), the S2p_{3/2} and S2p_{1/2} peaks being observed at 169.69 and 170.87 eV [13].

The binding energies of Pb 4f_{5/2} (between 139.19 and 139.35 eV) and 4f_{7/2} (between 144.07 and 144.23 eV) (Figures S8e and S9e, ESI) evidence the presence of PbCO₃, i.e., the synthetic white correspondent of the mineral cerussite [25]. Furthermore, the presence of Pb within one analyzed sample (Figure S10e, ESI) may be also correlated with the occurrence of PbO, (4f_{7/2} 138.35 eV, 4f_{5/2} 143.23 eV) [26], PbS, Pb(OH)₂ (4f_{7/2} 138.6 eV, 4f_{5/2} 143.48 eV), and PbSO₄ (4f_{7/2} 139.55 eV, 4f_{5/2} 144.43 eV) [13] species. The O 1s spectra related to the occurrence of PbO [3] and Pb(OH)₂ [27] could be observed at 530.38 and 532.24 eV, respectively. The presence of two peaks situated at 780.62 and 795.95 eV may be ascribed to BaSO₄ (Figure S10d, ESI) [22] (p. 139). The 2p_{3/2} and 2p_{1/2} components of sulfur illustrated the presence of PbS (161.25 eV, 162.43 eV) [13], elemental sulfur (163.71 eV, 164.89 eV) [28], adsorbed SO₂ (167 eV, 168.18 eV) [29] and PbSO₄ [22] (p. 189), CaSO₄ [22] (p. 69), and BaSO₄ [22] (p. 139) (169.69 eV, 170.87 eV) [12] species. The higher binding energy of oxygen centered between 531.84 and 532.33 eV can be also connected to chemisorbed oxygen [30].

3.3. Raman Spectroscopy

The Raman spectra of the representative pigments, impurities, and inks identified throughout the analysis of both the paintings and the micro-samples are illustrated in Figure 4 (portable Raman) and Figure 5 (μRaman). The assignments of the absorption bands (portable Raman) of the *Roses* and *Chrysanthemums* paintings, and of the absorption bands (μ-Raman) of the LIB, LIB_V, LIIA, LIIA_V, LIIA_pz1, and LIIA_pz2 samples, can be found in Tables S3 and S4 (ESI).

The portable Raman spectroscopy analyses (Figure 4) evidenced the use of several pigments, such as barium white (BaSO₄), vermilion, lead white, zinc white (ZnO), alizarin crimson, and strontium yellow, as well as beeswax. The dominant Raman bands illustrating the presence of barium white (*Roses*—analysis points 3, 5, 7, 8, 11, 18) were evidenced at 453 cm⁻¹ (ν₁ symmetric bending of SO₄²⁻), 462 cm⁻¹ (ν₂ bending of SO₄²⁻), and 989 cm⁻¹ (ν₁ symmetric stretching of SO₄²⁻), respectively [31]. The appearance of Raman bands at 253 cm⁻¹ (A1 mode), 283, and 343 cm⁻¹ (Eu mode) (*Roses*—analysis points 1, 4, 5, 6, 12, 15) can be associated with the HgS stretching modes of cinnabar, a natural red HgS mineral [32]. However, the absence of the Raman bands that may come from the presence of quartz, an impurity frequently found in association with cinnabar minerals, rather suggests the use of an artificial red pigment, i.e., vermilion. The use of zinc white (*Roses*—analysis point 6) was confirmed by the Raman bands at 386 cm⁻¹ (A1(TO) mode) and 435 cm⁻¹ (E2 mode),

respectively [33]. The presence of the orange pigment called alizarin crimson (PR83), i.e., 1,2-dihydroxyanthraquinone precipitated on aluminum hydrate (*Roses*—analysis point 14; *Chrysanthemums*—analysis point 9), was suggested by the intense Raman bands situated at 1291 cm^{-1} (CO stretching, CC stretching, CCC in-plane bending), 1327 cm^{-1} (CC stretching), and 1482 cm^{-1} (CO stretching, CC stretching, CH in-plane bending), respectively [34]. Due to the fluorescence phenomenon, the identification of some pigments through Raman spectroscopy was possible only based on the presence of a single band, i.e., the most intense one corresponding to each compound. The Raman peaks at 863 and 892 cm^{-1} (*Chrysanthemums*—analysis points 13, 14) correspond to the ν_1 symmetric and ν_3 antisymmetric stretching modes of the CrO_4 group from SrCrO_4 , i.e., a pale yellow pigment, also known under the name of strontium yellow [35]. Regarding the use of hydrocerussite, the Raman spectroscopy (*Chrysanthemums*—analysis points 8, 11, 12, 18) confirmed its presence through bands situated at 1049 cm^{-1} ($\nu_1\text{ CO}_3^{2-}$ symmetric stretching vibrations) and 1372 cm^{-1} ($\nu_3\text{ CO}_3^{2-}$ antisymmetric stretching vibrations) [36]. As opposed to the characteristic spectrum of hydrocerussite, no splitting of the ν_1 Raman band was recorded in the present study, most likely due to the formation of a new carbonate species, i.e., $x\text{PbCO}_3 \cdot y\text{PbS}$, under the action of atmospheric H_2S [37]. Although the presence of two Raman bands at 1298 cm^{-1} ($\delta(\text{CH}_2, \text{CH}_3)$ deformations) and 1442 cm^{-1} ($\delta(\text{CH}_2)$ deformations), respectively (*Chrysanthemums*—analysis point 8), can be correlated with the presence of either linseed oil, beeswax, shellac, or colophony [38], the absence of the strong Raman peak from around 1650 cm^{-1} might indicate the presence of only beeswax.

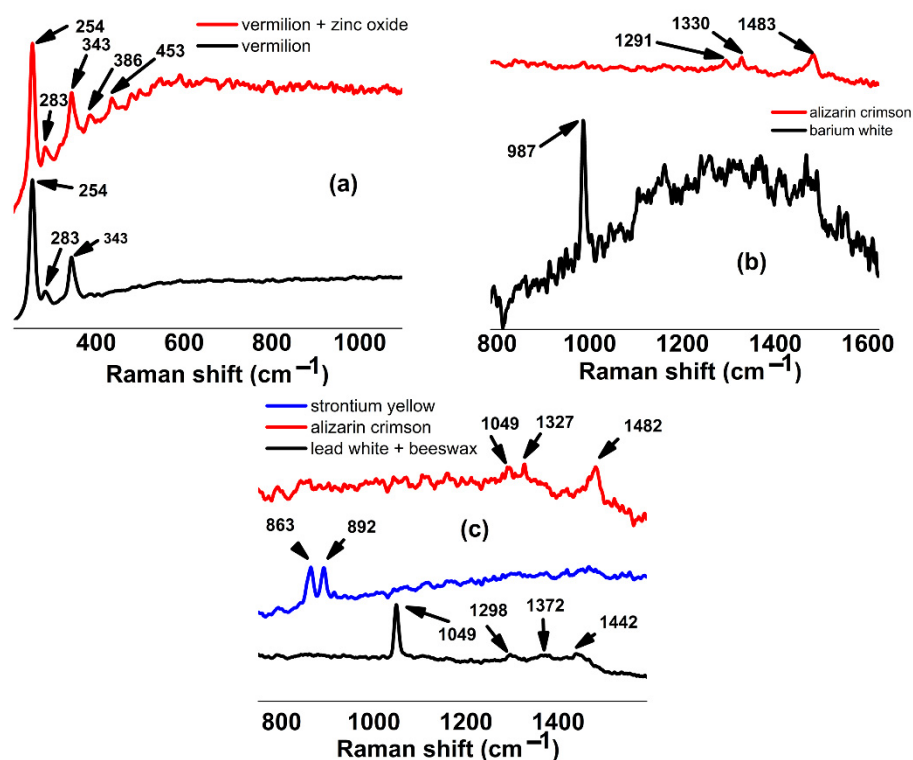


Figure 4. Portable Raman spectra of representative pigments, inks, and consolidating paint layers found at the analyzed points: (a) vermilion and zinc white, (b) alizarin crimson PR 83 and barium white (*Roses*), and (c) strontium yellow, alizarin crimson, lead white, and beeswax (*Chrysanthemums*).

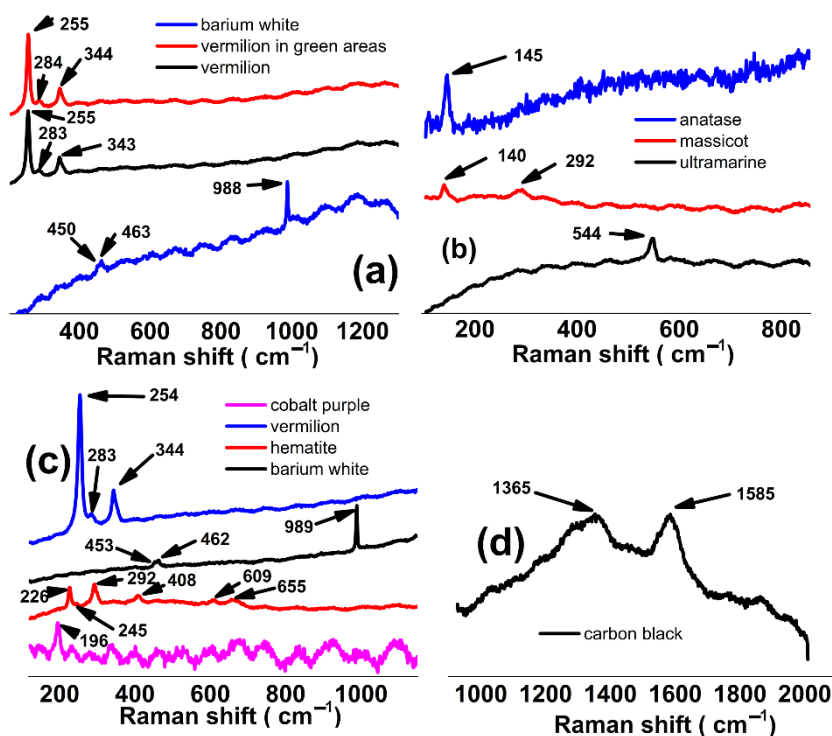


Figure 5. Micro-Raman spectra of representative pigments and impurities found at the analyzed points: (a) barium white and vermilion (*Roses*); (b) anatase, massicot, and ultramarine; (c) cobalt purple, vermilion, hematite, and barium white; and (d) carbon black (*Chrysanthemums*).

Either due to fluorescence or to the thick layer of linseed oil, in the case of *Roses*, only two pigments (barium white—LIB, vermilion—LIB, LIB_V) were evidenced in the μ Raman spectra (Figure 5). The analysis of *Chrysanthemums* allowed laser-induced degradation during Raman analysis, i.e., the identification of a large number of pigments and impurities in the LIIA sample (ultramarine, massicot, barium white, hematite, vermilion, cobalt purple, carbon black, and anatase). The presence of synthetic ultramarine was evidenced through only one Raman band at 544 cm^{-1} , which can be ascribed to the ν_1 symmetric stretching vibration of the S^{3-} ion [39]. The Raman analysis yielded, through the presence of bands at 140 cm^{-1} (combination band) and 292 cm^{-1} (B_{2g} and B_{3g}), respectively, evidence of the presence of massicot (orthorhombic PbO), a soft yellow pigment widely used since antiquity [40]. Although the use of massicot itself cannot be ruled out, this compound can also be found in red lead pigment (Pb_3O_4), either as an impurity or due to incomplete synthesis [9]. Although the misidentification of lead-based compounds (especially if these could derive from lead white degradation), can be encountered due to laser-induced degradation during Raman analysis, i.e., the degradation of plattnerite (PbO_2 , a dark brown to black pigment) into massicot at the operating Raman wavelength of 632.8 nm , the yellow color of the analyzed fragment eliminates this possibility [41]. The Raman bands placed at 226 cm^{-1} (A_{1g} mode, symmetric bends of Fe-O), 245 , 292 , 408 , 609 cm^{-1} (E_g mode, symmetric stretch of Fe-O), and 655 cm^{-1} (Eu mode, IR active LO) indicate the presence of hematite ($\alpha\text{-Fe}_2\text{O}_3$) [42], most likely as a constituent of a red ochre pigment. The presence of the Raman band located at 196 cm^{-1} can be attributed to the external mode of cobalt phosphate ($\text{Co}(\text{PO}_4)_2$), a dark cobalt violet pigment [43]. Raman spectroscopy alone is not able to discriminate between cobalt phosphate and its octahydrate form, i.e., $\text{Co}_3(\text{PO}_4)_2 \cdot 8\text{H}_2\text{O}$, another cobalt violet that was available at the time of the paintings' production. The micro-Raman spectra of several microscopic fragments showed the presence of two peaks, one located at 1365 cm^{-1} (D1 band, due to the occurrence of disordered structures, i.e., breathing modes of sp^2 bonded carbon atoms possessing A_{1g}

symmetry), and another one positioned at 1585 cm^{-1} (G band coming from the sp^2 carbon planar configuration of graphite, i.e., E_{2G2} vibration mode of a crystal with D_{6h}^4 symmetry) that can be ascribed to graphite, the crystalline form of carbon black, a generic term used to illustrate the presence of a carbon-based pigment [44]. One of the recorded spectra revealed the presence of anatase, with the B1g band at 145 cm^{-1} [45]. As anatase is not a pigment, but rather a component of another pigment, such as red ochre or yellow ochre, or a degradation product of titanium white (rutile), its presence cannot be definitively attributed to any specific source. However, the identification of hematite suggests that it is more likely present as a distinct grain within red ochre.

Despite repeated efforts to show the presence of indium yellow by means of μRaman spectroscopy, the measurements did not provide any useful spectra.

3.4. FTIR Spectroscopy

FTIR spectroscopy allowed use to acquire molecular information complementary to the ones obtained with the other analytical techniques, and increased our insight into the materials' composition and execution technique. The infrared spectra of the constitutive pigments and materials and details regarding the identification of the main absorption bands are shown in Figure 6. The assignments of absorption bands (FTIR) for the LIB, LIB_V, LIIA, LIIA_pz1, and LIIA_pz2 samples can be found in Table S5 (ESI). The absorption bands found in the FTIR spectra were mainly assigned by making reference to the presence of the absorption bands for the pigments that were already found through the other studied techniques, i.e., Raman, XPS, and EDS.

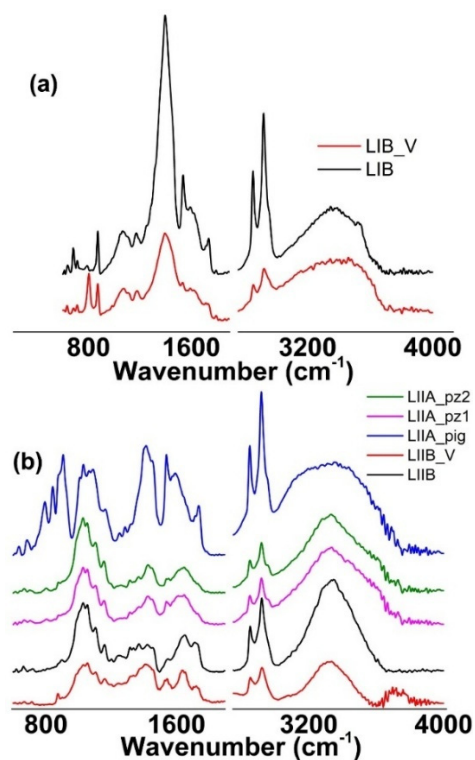


Figure 6. FTIR spectra of various samples: (a) LIB—microscopic sample from *Roses* painting, and LIB_V—microscopic sample with green hue from *Roses* painting; (b) LIIA—microscopic sample from *Chrysanthemums* painting, LIIA_V—microscopic sample with green hue from *Chrysanthemums* painting, LIIA—pigment area from canvas fragment from *Chrysanthemums* painting, LIIA_pz1—canvas area from canvas fragment from *Chrysanthemums* painting, and LIIA_pz2—canvas area from canvas fragment from *Chrysanthemums* painting.

Lead white pigment consists of a mixture of hydrocerussite ($\text{Pb}_3(\text{CO}_3)_2(\text{OH})_2$) and cerussite (PbCO_3) in various proportions [46], and was encountered in the LIB, LIB_V, and LIIA spectra. The FTIR spectrum of cerussite contained several absorption bands situated between 1730 and 1736 cm^{-1} ($\nu_1 + \nu_4$ combination modes of CO_3^{2-}), 1396 and 1400 cm^{-1} (antisymmetric stretching of CO_3^{2-}), 1053 and 1055 cm^{-1} (symmetric stretching of CO_3^{2-}), 842 and 849 cm^{-1} (out-of-plane bending vibration of CO_3^{2-}), and 680 and 685 cm^{-1} (in-plane bending vibration of CO_3^{2-}) [47]. As for hydrocerussite, several absorption bands could be observed at 3528 cm^{-1} (stretching mode of OH group), between 1730 and 1736 cm^{-1} ($\nu_1 + \nu_4$ combination modes of CO_3^{2-}), between 1396 and 1400 cm^{-1} (antisymmetric stretching of CO_3^{2-}), between 1053 and 1055 cm^{-1} (symmetric stretching of CO_3^{2-}), at 1045 cm^{-1} (symmetric stretching of CO_3^{2-}), between 930 and 931 cm^{-1} (δ Pb-OH), between 698 and 703 cm^{-1} (in-plane bending modes of CO_3^{2-}), and between 680 and 685 cm^{-1} (in-plane bending modes of CO_3^{2-}).

The absorption bands of strontium yellow (SrCrO_4), found in spectra LIIA, were located between 930 and 931 cm^{-1} , between 897 and 902 cm^{-1} , at 886 cm^{-1} , and between 872 and 879 cm^{-1} , corresponding to the Cr-O asymmetric stretching mode, while the ones situated between 842 and 849 cm^{-1} can be ascribed to Cr-O symmetric stretching mode [48].

The presence of quartz in the LIIA spectrum was evidenced by the appearance of the characteristic absorption bands located at 1165 cm^{-1} (Si-O asymmetrical stretching), at 1088 cm^{-1} (Si-O stretching), at 793 and 766 cm^{-1} (Si-O symmetrical stretching), and at 698 cm^{-1} (Si-O symmetrical bending) [49]. Besides red ochre, quartz can be frequently found as an associated material with other types of pigments, i.e., black chalk (graphite), calcium carbonate, kaolin, cinnabar, clay minerals, green earth, and lead white a.s.o. [9].

The occurrence of the absorption bands in the LIIA spectrum located at 3393 cm^{-1} ("loosely bound water" adsorbed on the surface), 3143 cm^{-1} (hydroxyl stretching), the triplet around 1697 cm^{-1} , 1646 cm^{-1} , and 1633 cm^{-1} (OH bending modes), 905 cm^{-1} (in-plane OH deformational mode), 793 cm^{-1} (out-of-plane OH deformational mode), 662 cm^{-1} (combination band), and 610 cm^{-1} (FeO_6 lattice) points out the presence of goethite ($\alpha\text{-FeOOH}$) [33] as a main constituent of yellow ochre pigment, i.e., a mixture of $\alpha\text{-FeOOH}$ and kaolinite. The absorption bands of kaolinite can be found in LIB_V at 3727 and 3662 cm^{-1} (outer hydroxyl ions), 3622 cm^{-1} (inner hydroxyl ions), 1023 cm^{-1} (Si-O-Si stretching), 1004 cm^{-1} (Si-O-Al stretching), 930 cm^{-1} (OH deformation, associated with 2Al^{3-}), and 776 and 793 cm^{-1} (symmetric stretching of Si-O-Si inter tetrahedral bonds) [50]. The main coloring component of red ochre is hematite, which may usually be found in association with calcite, ilmenite, magnetite, feldspars, and rutile, and is sometimes adulterated with quartz [9]. Hematite has no characteristic absorption bands in the $4000\text{--}6000\text{ cm}^{-1}$ range.

The main absorption band of cobalt phosphate ($\text{Co}_3(\text{PO}_4)_2$), i.e., the antisymmetric stretching, is located at 1045 cm^{-1} , accompanied by two other shoulders between 1064 and 1067 cm^{-1} and 1028 and 1030 cm^{-1} , respectively (LIB, LIIA). Other characteristic absorption bands can be found between 945 and 953 cm^{-1} and 633 and 637 cm^{-1} (bending of O-P-O group), as well as between 984 and 985 cm^{-1} (P-O stretching) and 680 and 685 cm^{-1} (Co-O lattice vibration mode), respectively. The presence of the crystallization water of $\text{Co}_3(\text{PO}_4)_2$ is indicated by the OH stretching vibration at around 3080 cm^{-1} and by the H-OH bending vibration at 1593 cm^{-1} [51].

While several other pigments, such as viridian [52], barium white [53], CdS [54], cobalt green or Rinnemann's green pigment [55], and ultramarine [56] were identified through the other spectroscopic techniques, and all their characteristic absorption bands were present within the FTIR spectra, the overlapping of the absorption bands makes their clear identification problematic. The same situation was encountered for beeswax (a

consolidating paint layer) [57] and shellac resin [58,59]. The assignment of the absorption bands corresponding to these pigments can be found in Table S5 (ESI).

The absorption bands from around 1336 cm^{-1} (CH_2 deformation band, LIIB, LIIB_V, LIIA_pz1 and LIIA_pza2) indicate the use of an animal glue as a proteinaceous binder in the studied oil painting. The positions of the CH_2 deformation band ($\sim 1336\text{ cm}^{-1}$) and of absorption bands that can be correlated with the presence of amide I (between 1625 and 1627 cm^{-1}), amide II (between 1527 and 1532 cm^{-1}), and amide III (1237 – 1241 cm^{-1}), are characteristic of protein-based materials, mainly collagen-derived glues such as rabbit skin, hide, and bone glues [60–62]. However, due to the similar absorption band positions for amide I, II, and III and CH_2 deformation for all animal glues, and the overlap of other absorption bands within the same region, the FTIR technique cannot identify the specific type of animal glue.

The fundamental vibration modes of gypsum ($\text{CaSO}_4 \cdot 2\text{H}_2\text{O}$) may be observed between 3385 and 3393 cm^{-1} (OH stretching), 2087 and 2091 cm^{-1} (combination of 1st overtone and asymmetric stretching of SO_4^{2-}), 1156 and 1165 cm^{-1} (symmetric bending of SO_4^{2-}), 1003 and 1008 cm^{-1} (symmetric stretching of SO_4^{2-}), 876 and 879 cm^{-1} (OH bending), 677 and 685 , and 610 and 611 cm^{-1} (asymmetric bending of SO_4^{2-}), respectively (LIIA, LIIB_V, LIIA_pz1, and LIIA_pz2) [63].

Calcium carbonate was found in the spectra of LIB, LIB_V, LIIA_pz1, and LIIA_pz2, and its presence can be attributed either to its use as a filler or its presence as an impurity in ochres. The vibrations of calcium carbonate can be found between 1786 and 1792 cm^{-1} (stretching of CO_3^{2-}), 1421 and 1432 cm^{-1} (asymmetric stretching of CO_3^{2-}), 872 and 879 cm^{-1} (out-of-plane bending of CO_3^{2-}), and 712 and 715 cm^{-1} (planar bending of CO_3^{2-}) [64].

3.5. Degradation Processes

The occurrence of both carboxylic acids and metal carboxylates indicates a degradation process. Whereas carboxylic acids appear due to degradation processes in drying oil, metal carboxylates migrate to the painting's surface and form protrusions, i.e., clusters of metal soaps, that are responsible for various deterioration phenomena, such as susceptibility to mechanical damage, loss of pigment, modification of light areas as a consequence of dirt incorporation or changes in fatty acid ratios, and changes in surface texture [64].

The main absorption bands that can be attributed to aged linseed oil can be seen between 3332 and 3340 cm^{-1} (OH stretching of oxidative products such as hydroperoxides, alcohols), 2918 and 2922 cm^{-1} (asymmetric CH stretching of alkyl CH-CH_2 groups), 2851 and 2853 cm^{-1} (symmetric CH stretching of CH-CH_2 and CH_3 groups), 2729 and 2740 cm^{-1} (overtone CH in plane deformation of aliphatic aldehydes), 1730 and 1735 cm^{-1} (ester C=O stretching of triglyceride constituents), 1712 and 1714 cm^{-1} (C=O stretching of free carboxylic acids and saturated ketones appeared upon oxidation), 1643 and 1654 cm^{-1} (C=C stretching, C=O stretching of aldehyde or acid compounds), 1611 and 1613 cm^{-1} (C=O stretching of carboxylic acids, aldehydes, α/β unsaturated ketones), 1454 and 1460 cm^{-1} (CH_3 asymmetric bending and CH_2 scissoring), 1406 and 1414 cm^{-1} (CO bending of acid groups, CH bending of $-\text{CH}_2-\text{COO}$ groups), 1370 and 1373 cm^{-1} (CH bending), 1234 and 1241 cm^{-1} (CH_2 twisting of esters), 1249 and 1260 , 1156 and 1165 , and 1103 and 1105 cm^{-1} (CO stretching in C-O-C groups from esters), 1200 and 1202 cm^{-1} (CO stretching from alcohols), and 984 and 986 cm^{-1} (CH wagging of isolated trans CH=CH groups), respectively [65]. The absence of the absorption band from around 3010 cm^{-1} , representing CH stretching of the aliphatic cis un-conjugated double bonds, can be connected with the cis-trans isomerization reaction of linseed oil as a result of oxidation and polymerization during drying. The isomerization process is usually accompanied by the disappearance of CH

bending of the aliphatic cis un-conjugated double bonds (between 719 and 724 cm^{-1} —not clearly evidenced in the present study due to the overlapping of other absorption bands), as well as by the increase in the absorption bands between 984 and 986 cm^{-1} , representing CH wagging of isolated trans CH=CH groups. The lower intensity of these absorption bands, in comparison with the ones belonging to asymmetric stretching vibrations of carboxylate groups, points out the hydrolysis of the ester groups from triglycerides and formation of metal carboxylates. The position of the asymmetric stretching vibrations of carboxylate groups from metal soaps depends on the type of the metal ion, i.e., between 1593 and 1597 cm^{-1} (copper oleates, LIIB, LIIB_V), 1574 and 1576 cm^{-1} (calcium palmitates, LIB, LIB_V, LIIB_pz1, LIIB_pz2), 1564 cm^{-1} (manganese palmitates, LIIB_V), 1538 and 1546 cm^{-1} (lead palmitates, LIIB, LIIB_V, LIIB_pz1, LIIB_pz2), 1485 and 1492 cm^{-1} (lead oleates, LIIB_V, LIIB_pz1, LIIB_pz2), and 1538 and 1544 cm^{-1} (zinc oleates, LIIB, LIIB_V) [66]. Symmetric stretching vibrations of carboxylate units for copper, calcium, and manganese metal ions may be observed between 1421 and 1432 cm^{-1} , while for zinc and lead, these appeared between 1404 and 1414 cm^{-1} , and between 1406 and 1412 cm^{-1} , respectively. CH_2 bending vibrations can be noticed in the 1452 and 1458 cm^{-1} range for all metal cations.

Among the pigments already found in the studied samples that are usually subjected to chemical degradation or fading, one can mention lead-based pigments. The degradation of lead white is usually described as a blackening process due to the formation of galena (PbS), although different types of colors, i.e., ranging from light pink to black, can result under the action of atmospheric hydrogen sulfides or interaction with other sulfur-containing pigments. Although no significant darkening of the painting surfaces was observed in the present study, most likely because the artist used a low concentration of lead white pigment, some evidence regarding the blackening process of lead white was obtained through XPS and Raman and FTIR spectroscopies. XPS evidenced the presence of the oxidation products of galena (PbS) upon exposure to air, i.e., PbO, Pb(OH)₂, PbSO₄, and elemental sulfur [67]. The appearance of a new carbonate species, i.e., xPbCO₃·yPbS, in one Raman spectrum, illustrated a change in the color appearance of lead white pigment. The absence of PbS in the corresponding Raman spectrum can be related to either the fluorescence phenomenon or to a partial protection offered by the frames against the H₂S action, since the micro-samples subjected to spectral analyses were collected from under the frames. As concerns the FTIR spectra, the decomposition of galena in acidic conditions usually yields PbSO₄ [9]. PbSO₄ displays several components of asymmetric and symmetric stretching modes of SO₄²⁻ between 1173 and 1179 cm^{-1} , 1053 and 1054 cm^{-1} , and 945 and 956 cm^{-1} , respectively, as well as asymmetric bend modes of SO₄²⁻ between 633 and 643 cm^{-1} [60]. The only structural changes that may be correlated with lead white darkening over time can be highlighted in the monitoring of the evolution of the absorption bands located at 3528 cm^{-1} (OH stretching), between 1394 and 1400 cm^{-1} (C-O stretching), and between 680 and 685 cm^{-1} (in-plane bending modes of CO₃²⁻), respectively [68]. Due to the overlapping of the absorption bands of lead white with the ones corresponding to the linseed oil, the decrease in only one absorption band, i.e., the one situated between 680 and 685 cm^{-1} , illustrates changes in the C-O groups linked to Pb due to their replacement with sulfide units.

The main absorption bands correlated with asymmetric C=O stretching of copper and zinc oxalates are situated between 1666 and 1673 cm^{-1} (LIB_V, LIIB, LIIB_V) and between 1629 and 1635 cm^{-1} [69] (LIIB, LIIB_V), respectively. The other absorption bands of copper oxalate can be viewed at 1364 cm^{-1} and between 1315 and 1319 cm^{-1} (combination modes of C-O stretching and O-C=O bending). As regards zinc oxalates, the other absorption bands of zinc oxalates appeared around 3390 cm^{-1} (OH stretching), and between 1370–1373 and

1315–1316 cm^{-1} (combination modes of C–O stretching and O–C=O bending), respectively. Most likely, the formation of both copper and zinc oxalates can be connected with the selective chemical degradations of a copper-containing pigment and zinc white in the presence of an oxalic acid source [70], i.e., a degraded lipidic paint binder exposed to UV irradiation and air pollutants [71]. The absence of the malachite strong absorption band that usually appears at 1494 cm^{-1} suggests the lack of green malachite pigment, therefore the copper green pigment may be verdigris or copper resinate.

Taking into account the level of some pigment's degradation, the conservation and restoration of the two heritage artworks, i.e., *Chrysanthemums* and *Roses*, are necessary. Furthermore, other measures to assure long-term protection can be considered, such as the use of a UV-blocking glass or of particular LED sources containing a tunable white lighting technology.

4. Conclusions

The identification and the structural characterization of materials and pigments used by the great artist Stefan Luchian in two important cultural heritage paintings illustrate the painter's preference for a high variety of pigments of red, yellow, and green colors, a common practice of post-impressionism painters. The incidence of a degradation process of some of the pigments used, i.e., lead white and a copper-containing pigment, was demonstrated by the appearance of the oxidation products and variation in some absorption bands from FTIR or Raman spectra. Furthermore, evidence concerning the presence of metal soaps and carboxylic acids completed the overall picture of the degradation phenomena.

This article is the first to provide information regarding the use of In_2O_3 as a yellow pigment in artwork. The lack of information does not necessarily mean that this metal oxide was not previously used as a yellow pigment by other painters. This could be attributed to several factors, like the use of small amounts in masterpieces, the inhomogeneity of works of art, or being simply the fact of it being overlooked up to this point due to a very small number of references in the literature. At the same time, the presence of K in works of art may cause researchers performing XRF measurements in museum settings, who are not acquainted with the literature on In-based pigments, to disregard the presence of In_2O_3 in their measurements, and attribute the signal to K. The identification of In_2O_3 was demonstrated through SEM/EDS and XPS techniques that prove to be valuable tools for the identification of the presence of indium oxide when it is possible to take microscopic fragments from under picture frames.

Supplementary Materials: The following supporting information can be downloaded at <https://www.mdpi.com/article/10.3390/heritage8010026/s1>: Figure S1: Investigated cadmium yellow grain: (a) optical microscopy, (b) SEM image of the investigated area (as identified on the basis of sample morphology and optical microscopy) with the pigment grain highlighted, (c) EDS spectrum of the investigated grain revealing high amounts of Cd and S; Figure S2: Investigated Prussian blue grain: (a) optical microscopy, (b) SEM image of the investigated area (as identified on the basis of sample morphology and optical microscopy) with the pigment grain highlighted, (c) EDS spectrum of the investigated grain revealing high amounts of Fe.; Figure S3: Investigated cobalt purple grain: (a) optical microscopy, (b) SEM image of the investigated area (as identified on the basis of sample morphology and optical microscopy) with the pigment grain highlighted, (c) EDS spectrum of the investigated grain showing significant amounts of Co and P; Figure S4: Investigated chrome green grain: (a) optical microscopy, (b) SEM image of the investigated area (as identified on the basis of sample morphology and optical microscopy) with the pigment grain highlighted, (c) EDS spectrum of the investigated grain exhibiting high amounts of Cr; Figure S5: Investigated green copper grain: (a) optical microscopy, (b) SEM image of the investigated area (as identified on the basis of sample morphology and optical microscopy) with the pigment grain highlighted, (c) EDS spectrum of the

investigated grain showing high amounts of Cu; Figure S6: XPS spectra of relevant elements—sample from *Chrysanthemums* painting, sample LIIA—canvas fragment with black smudges. Spectrum was recorded from pigment area—blackish smudges (LIIA): (a) C 1s spectrum and peak fitting, (b) Co 2p spectrum and peak fitting, (c) O 1s spectrum and peak fitting, (d) Zn 2p spectrum and peak fitting; Figure S7: XPS spectra of relevant elements—sample from *Chrysanthemums* painting, sample LIIA—canvas fragment with black smudges. Spectrum was recorded from canvas area (LIIA): (a) C 1s spectrum and peak fitting, (b) N 1s spectrum and peak fitting, (c) O 1s spectrum and peak fitting, (d) Zn 2p spectrum and peak fitting; Figure S8: XPS spectra of relevant elements—sample from *Roses* painting, sample LIB—small grains: (a) C 1s spectrum and peak fitting, (b) O 1s spectrum and peak fitting, (c) Ca 2p spectrum and peak fitting, (d) Si 2p spectrum and peak fitting, (e) Pb 4f spectrum and peak fitting; Figure S9: XPS spectra of relevant elements—sample from *Chrysanthemums* painting, sample LIIB—small grains: (a) C 1s spectrum and peak fitting, (b) O 1s spectrum and peak fitting, (c) Zn 2p spectrum and peak fitting, (d) Ca 2p spectrum and peak fitting, (e) Pb 4f spectrum and peak fitting; Figure S10: XPS spectra of relevant elements—sample from *Chrysanthemums* painting, sample LIIA—canvas fragment with black smudges. Spectrum was recorded from pigment area—blackish smudges (LIIA): (a) C 1s spectrum and peak fitting, (b) O 1s spectrum and peak fitting, (c) Ca 2p spectrum and peak fitting, (d) Ba 3d spectrum and peak fitting, (e) Pb 4f spectrum and peak fitting, (f) S 2p spectrum and peak fitting, (g) Zn 2p spectrum and peak fitting.

Author Contributions: Conceptualization, M.G. and L.S.; methodology, A.V.O. and B.S.; validation, A.V.O.; investigation, L.E.U., M.M., M.D. and A.V.O.; resources, M.G.; writing—original draft preparation, M.O. and A.V.O.; writing—review and editing, M.O., B.S., L.S. and A.V.O.; visualization, A.V.O.; supervision, L.S. and B.S.; project administration, M.O. and A.V.O. All authors have read and agreed to the published version of the manuscript.

Funding: This research received no external funding.

Data Availability Statement: The data supporting this study are available upon request from the corresponding author.

Acknowledgments: We want to thank Simion Aștilean, from the NanoBioPhotonics and Laser Microspectroscopy Center within the Interdisciplinary Research Institute in Bio-Nano-Sciences, Cluj, Romania, for the use of a portable Raman spectrophotometer (R-3000CN from Raman Systems).

Conflicts of Interest: The authors declare no conflicts of interest.

References

1. Drăguț, V.; Florea, V.; Grigorescu, D.; Mihalache, M. *Pictura Românească în Imagini*; Meridiane: Bucharest, Romania, 1970; pp. 168–179.
2. Stefan Luchian-Anemone. Available online: <https://ro.scribd.com/doc/55179121/Anemone-2#> (accessed on 12 June 2024).
3. Geba, M.; Stratulat, L.; Vornicu, N.; Salajan, D.; Manea, M.M. Research on the chromatic palette of a modern Romanian painter. *Rev. Chim.* **2017**, *68*, 447–452. [CrossRef]
4. Field, G. *Field's Chromatography: Or, Treatise on Colours and Pigments as Used by Artists*; Salter, T.W., Ed.; Winsor and Newton: London, UK, 1869; pp. 115–118.
5. Smith, A.E.; Mizoguchi, H.; Delaney, K.; Spaldin, N.A.; Sleight, A.W.; Subramanian, M.A. Mn^{3+} in trigonal bipyramidal coordination: A new blue chromophore. *J. Am. Chem. Soc.* **2009**, *131*, 17084–17086. [CrossRef] [PubMed]
6. Watts, J.F.; Wolstenholme, J. *An Introduction to Surface Analysis by XPS and AES*; Chapter 1; John Wiley & Sons Ltd.: Chichester, UK, 2003; pp. 1–18. [CrossRef]
7. Astolfi, M.L. Advances in analytical strategies to study cultural heritage samples. *Molecules* **2023**, *28*, 6423. [CrossRef] [PubMed] [PubMed Central]
8. Madariaga, J.M. Analytical chemistry in the field of cultural heritage. *Anal. Methods* **2015**, *7*, 4848–4876. [CrossRef]
9. Eastaugh, N.; Walsh, V.; Chaplin, T.; Siddall, R. *Pigment Compendium, A Dictionary and Optical Microscopy of Historical Pigments*; Elsevier: Oxford, UK, 2008; ISBN 9780750689809.
10. Monico, L.; Van der Snickt, G.; Janssens, K.; De Nolf, W.; Miliani, C.; Dik, J.; Radepon, M.; Hendriks, E.; Geldof, M.; Cottez, M. Degradation process of lead chromate in paintings by Vincent van Gogh studied by means of synchrotron X-ray spectromicroscopy and related methods. 2. Original paint layer samples. *Anal. Chem.* **2011**, *83*, 1224–1231. [CrossRef]

11. Greczynski, G.; Hultman, L. C 1s peak of adventitious carbon aligns to the vacuum level: Dire consequences for material's bonding assignment by photoelectron spectroscopy. *ChemPhysChem* **2017**, *18*, 1507–1512. [CrossRef]
12. Du, N.; Zhang, H.; Chen, B.; Ma, X.; Liu, Z.; Wu, J.; Yang, D. Porous indium oxide nanotubes: Layer-by-layer assembly on carbon-nanotube templates and application for room-temperature NH₃ gas sensors. *Adv. Mater.* **2007**, *19*, 1641–1645. [CrossRef]
13. NIST X-Ray Photoelectron Spectroscopy (XPS) Database. Available online: <https://srdata.nist.gov/xps/> (accessed on 19 December 2024).
14. Sano, N.; Cumpson, P.J.; Cwiertnia, E.; Perry, J.J.; Singer, B.W. Multivariate analysis studies of the ageing effect for artist's oil paints containing modern organic pigments. *Surf. Interface Anal.* **2014**, *46*, 786–790. [CrossRef]
15. Thiel, A.; Luckmann, H.Z. Studien über das Indium. III. Abhandlung. *Z. Anorg. Allg. Chem.* **1928**, *172*, 353–371. [CrossRef]
16. Lawrence, R.E.; Westbrook, L.R. Indium-occurrence, recovery and uses. *Ind. Eng. Chem.* **1938**, *30*, 611–621. [CrossRef]
17. Nashim, A.; Martha, S.; Parida, K.M. Gd₂Ti₂O₇/In₂O₃: Efficient visible-light-driven heterojunction-based composite photocatalysts for hydrogen production. *ChemCatChem* **2013**, *5*, 2352–2359. [CrossRef]
18. Bartiaux, S.; Lhoest, J.-B.; Genet, M.J.; Bertrand, P.; Rouxhet, P.G. Poly(amino acids) by XPS: Analysis of poly(L-serine). *Surf. Sci. Spectra* **1994**, *3*, 342–347. [CrossRef]
19. Baltrusaitis, J.; Jayaweera, P.M.; Grassian, V.H. XPS study of nitrogen dioxide adsorption on metal oxide particle surfaces under different environmental conditions. *Phys. Chem. Chem. Phys.* **2009**, *11*, 8295–8305. [CrossRef] [PubMed]
20. Rasouli, S.; Moeen, S.J. Combustion synthesis of Co-doped zinc oxide nanoparticles using mixture of citric acid–glycine fuels. *J. Alloys Compd.* **2011**, *509*, 1915–1919. [CrossRef]
21. Gandhi, V.; Ganesan, R.; Syedahamed, H.H.A.; Thaiyan, M. Effect of cobalt doping on structural, optical, and magnetic properties of ZnO nanoparticles synthesized by coprecipitation method. *J. Phys. Chem. C* **2014**, *118*, 9715–9725. [CrossRef]
22. Moulder, J.F. *Handbook of X-Ray Photoelectron Spectroscopy: A Reference Book of Standard Spectra for Identification and Interpretation of XPS Data*; Perkin-Elmer Corporation: Eden Prairie, MN, USA, 1992; ISBN 0962702625/9780962702624.
23. Al-Gaashani, R.; Radiman, S.; Daud, A.R.; Tabet, N.; Al-Douri, Y. XPS and optical studies of different morphologies of ZnO nanostructures prepared by microwave methods. *Ceram. Int.* **2013**, *39*, 2283–2292. [CrossRef]
24. Tingle, T.N.; Borch, R.S.; Hochella, M.F.; Becker, C.H.; Walker, W.J. Characterization of lead on mineral surfaces in soils contaminated by mining and smelting. *J. Appl. Surf. Sci.* **1993**, *72*, 301–306. [CrossRef]
25. Baltrusaitis, J.; Usher, C.R.; Grassian, V.H. Reactions of sulfur dioxide on calcium carbonate single crystal and particle surfaces at the adsorbed water carbonate interface. *Phys. Chem. Chem. Phys.* **2007**, *9*, 3011–3024. [CrossRef]
26. Yoshida, T.; Yamaguchi, T.; Iida, Y.; Nakayama, S. XPS study of Pb(II) adsorption on γ -Al₂O₃ surface at high pH conditions. *J. Nucl. Sci. Technol.* **2003**, *40*, 672–678. [CrossRef]
27. Huang, W.; Sadhu, S.; Ptasinska, S. Heat- and gas-induced transformation in CH₃NH₃PbI₃ perovskites and its effect on the efficiency of solar cells. *Chem. Mater.* **2017**, *29*, 8478–8485. [CrossRef]
28. Smart, R.S.C.; Skinner, W.M.; Gerson, A.R. XPS of sulphide mineral surfaces: Metal-deficient, polysulphides, defects and elemental sulphur. *Surf. Interface Anal.* **1999**, *28*, 101–105. [CrossRef]
29. Furuyama, M.; Kishi, K.; Ikeda, S. The adsorption of SO₂ on iron surfaces studied by x-ray photoelectron spectroscopy. *J. Electron. Spectros. Relat. Phenom.* **1978**, *13*, 59–67. [CrossRef]
30. Chen, M.; Wang, X.; Yu, Y.H.; Pei, Z.L.; Bai, X.D.; Sun, C.; Huang, R.F.; Wen, L.S. X-ray photoelectron spectroscopy and auger electron spectroscopy studies of Al-doped ZnO films. *Appl. Surf. Sci.* **2000**, *158*, 134–140. [CrossRef]
31. White, S.N. Laser Raman spectroscopy as a technique for identification of seafloor hydrothermal and cold seep minerals. *Chem. Geol.* **2009**, *259*, 240–252. [CrossRef]
32. Frost, R.L.; Martens, W.N.; Klopogge, J.T. Raman spectroscopic study of cinnabar (HgS), realgar (As₄S₄), and orpiment (As₂S₃) at 298 and 77K. *N. Jb. Miner. Mh.* **2002**, *10*, 469–480. [CrossRef]
33. Prasad, P.S.R.; Shiva Prasad, K.; Krishna Chaitanya, V.; Babu, E.V.S.S.K.; Sreedhar, B.; Ramana Murthy, S. In situ FTIR study on the dehydration of natural goethite. *J. Asian Earth Sci.* **2006**, *27*, 503–511. [CrossRef]
34. Legan, L.; Retko, K.; Ropret, P. Vibrational spectroscopic study on degradation of alizarin carmine. *Microchem. J.* **2016**, *127*, 36–45. [CrossRef]
35. Scheuermann, W.; Ritter, G.J.; Schutte, C.J.H. The vibrational spectra of strontium chromate (SrCrO₄) and lead chromate (PbCrO₄). *Z. Naturforsch.* **1970**, *25*, 1856–1862. [CrossRef]
36. Ciomartan, D.A.; Clark, R.J.H.; McDonald, L.J.; Odlyha, M. Studies on the thermal decomposition of basic lead(II) carbonate by Fourier-transform Raman spectroscopy, X-ray diffraction and thermal analysis. *J. Chem. Soc. Dalton Trans.* **1996**, *18*, 3639–3645. [CrossRef]
37. Smith, G.D.; Clark, R.J.H. The role of H₂S in pigment blackening. *J. Cult. Herit.* **2002**, *3*, 101–105. [CrossRef]
38. Vandenabeele, P.; Wehling, B.; Moens, L.; Edwards, H.; De Reu, M.; Van Hooydonk, G. Analysis with micro-Raman spectroscopy of natural organic binding media and varnishes used in art. *Anal. Chim. Acta* **2000**, *407*, 261–274. [CrossRef]

39. Osticioli, I.; Mendes, N.F.C.; Nevin, A.; Gil, F.P.S.C.; Becucci, M.; Castellucci, E. Analysis of natural and artificial ultramarine blue pigments using laser induced breakdown and pulsed Raman spectroscopy, statistical analysis and light microscopy. *Spectrochim. Acta Part A Mol. Biomol. Spectrosc.* **2009**, *73*, 525–531. [[CrossRef](#)] [[PubMed](#)]
40. Donaldson, J.D.; Donoghue, M.T.; Ross, S.D. The vibrational spectra of tetragonal and orthorhombic PbO. *Spectrochim. Acta* **1974**, *30A*, 1967–1975. [[CrossRef](#)]
41. Smith, G.D.; Burgio, L.; Firth, S.; Clark, R.J.H. Laser-induced degradation of lead pigments with reference to Botticelli's Trionfo d'Amore. *Anal. Chim. Acta* **2001**, *440*, 185–188. [[CrossRef](#)]
42. Marshall, C.P.; Dufresne, W.J.B.; Ruffledt, C.J. Polarized Raman spectra of hematite and assignment of external modes. *J. Raman Spectrosc.* **2020**, *51*, 1522–1529. [[CrossRef](#)]
43. Casadio, F.; Bezúr, A.; Fiedler, I.; Muir, K.; Trad, T.; Maccagnola, S. Pablo Picasso to Jasper Johns: A Raman study of cobalt-based synthetic inorganic pigments. *J. Raman Spectrosc.* **2012**, *43*, 1761–1771. [[CrossRef](#)]
44. Ferrari, A.C.; Robertson, J. Interpretation of Raman spectra of disordered and amorphous carbon. *Phys. Rev. B* **2000**, *61*, 14095–14107. [[CrossRef](#)]
45. Taudul, B.; Tielens, F.; Calatayud, M. On the origin of Raman activity in anatase TiO₂ (nano) materials: An ab initio investigation of surface and size effects. *Nanomaterials* **2023**, *13*, 1856. [[CrossRef](#)]
46. Chevrier, C.; Giester, G.; Heger, G.; Jarosch, D.; Wildner, M.; Zemmann, J. Neutron single-crystal refinement of cerussite, PbCO₃, and comparison with other aragonite-type carbonates. *Z. Kristallogr. Cryst.* **1992**, *199*, 67–74. [[CrossRef](#)]
47. Brooker, M.H.; Sunder, S.; Taylor, P.; Lopata, V.J. Infrared and Raman spectra and X-ray diffraction studies of solid lead(II) carbonates. *Can. J. Chem.* **1983**, *61*, 494–502. [[CrossRef](#)]
48. Bharat, L.K.; Reddy, L.S.; Yu, J.S. Sol-gel synthesis, characterization and photocatalytic properties of SrCrO₄ particles. *Mater. Lett.* **2015**, *144*, 85–89. [[CrossRef](#)]
49. Udvardi, B.; Kovács, I.J.; Kónya, P.; Földvári, M.; Fűri, J.; Budai, F.; Falus, G.; Fancsik, T.; Szabó, C.; Szalai, Z.; et al. Application of attenuated total reflectance Fourier transform infrared spectroscopy in the mineralogical study of a landslide area, Hungary. *Sediment. Geol.* **2014**, *313*, 1–14. [[CrossRef](#)]
50. Ferreira, G.R.; Garcia, H.C.; Couri, M.R.C.; Dos Santos, H.F.; de Oliveira, L.F.C. On the azo/hydrazo equilibrium in Sudan I azo dye derivatives. *J. Phys. Chem. A* **2013**, *117*, 642–649. [[CrossRef](#)]
51. Corbeil, M.C.; Charland, J.P.; Moffatt, E.A. The characterization of cobalt violet pigments. *Stud. Conserv.* **2002**, *47*, 237–249. [[CrossRef](#)]
52. Subba Rao, G.V.; Rao, C.N.R.; Ferraro, J.R. Infrared and electronic spectra of rare earth perovskites: Ortho-chromites, -manganites and -ferrites. *Appl. Spectrosc.* **1970**, *24*, 436–445.
53. Prameena, B.; Anbalagan, G.; Sangeetha, V.; Gunasekaran, S.; Ramkumar, G.R. Behaviour of Indian natural baryte mineral. *Int. J. Chemtech Res.* **2013**, *5*, 220–231.
54. Muniyappan, S.; Arivunithi, V.; Solaiyammal, T.; Sudhakar, K.; Kumar, R.R.; Murugakoothan, P. Synthesis, structural, optical, morphological and elemental characterization of CTAB capped CdS quantum dots by facile chemical precipitation technique. In *Recent Trends in Materials Science and Applications*; Springer Proceedings in Physics 189: New York, NY, USA, 2017; pp. 341–348. [[CrossRef](#)]
55. Ashokkumar, M.; Muthukumar, S. Microstructure, optical and FTIR studies of Ni, Cu co-doped ZnO nanoparticles by co-precipitation method. *Opt. Mater.* **2014**, *37*, 671–678. [[CrossRef](#)]
56. Ostrooumov, M.; Fritsch, E.; Faulques, E.; Chauvet, O. Spectrometric study of lazurite from the Pamirs, Tajikistan. *Can. Mineral.* **2002**, *40*, 885–893. [[CrossRef](#)]
57. Shearer, G.L. An Evaluation of Fourier Transform Spectroscopy for the Characterization of Organic Compounds in Art and Archaeology. Ph.D. Thesis, University College London, London, UK, 1989.
58. Available online: http://lisa.chem.ut.ee/IR_spectra/coating_materials/shellac/ (accessed on 18 December 2024).
59. Ciofini, D. Removal of Varnish and Overpaint Layers from Easel Paintings Using Pulsed Nd:YAG Lasers. Ph.D. Thesis, Università degli Studi di Firenze, Florence, Italy, 2014.
60. Rabbitskin Glue. Available online: <https://spectra.chem.ut.ee/paint/binders/rabbitskin-glue/> (accessed on 18 December 2024).
61. Riaz, T.; Zeeshan, R.; Zarif, F.; Ilyas, K.; Muhammad, N.; Safi, S.Z.; Rahim, A.; Rizvi, S.A.A.; Rehman, I.U. FTIR analysis of natural and synthetic collagen. *Appl. Spectrosc. Rev.* **2018**, *53*, 703–746. [[CrossRef](#)]
62. Pellegrini, D.; Duce, C.; Bonaduce, I.; Biagi, S.; Ghezzi, L.; Colombini, M.P.; Tinè, M.R.; Bramanti, E. Fourier transform infrared spectroscopic study of rabbit glue/inorganic pigments mixtures in fresh and aged reference paint reconstructions. *Microchem. J.* **2016**, *124*, 31–35. [[CrossRef](#)]
63. Lane, M.D. Mid-infrared emission spectroscopy of sulfate and sulfate-bearing minerals. *Am. Min.* **2007**, *92*, 1–18. [[CrossRef](#)]
64. Higgitt, C.; Spring, M.; Saunders, D. Pigment-medium interactions in oil paint films containing lead-based pigments. *WAAC Newslett.* **2005**, *27*, 12–16.

65. Morsch, S.; Van Driel, B.A.; van den Berg, K.J.; Dik, J. Investigating the photocatalytic degradation of oil paint using ATR-IR and AFM-IR. *ACS Appl. Mater. Interfaces* **2017**, *9*, 10169–10179. [[CrossRef](#)] [[PubMed](#)]
66. Otero, V.; Sanches, D.; Montagner, C.; Vilarigues, M.; Carlyle, L.; Lopes, J.A.; Melo, M.J. Characterisation of metal carboxylates by Raman and infrared spectroscopy in works of art. *J. Raman Spectrosc.* **2014**, *45*, 1197–1206. [[CrossRef](#)]
67. Buckley, A.N.; Woods, R. An X-ray photoelectron spectroscopic study of the oxidation of galena. *App. Surf. Sci.* **1984**, *17*, 401–414. [[CrossRef](#)]
68. Goltz, D.; McClelland, J.; Schellenberg, A.; Attas, M.; Cloutis, E.; Collins, C. Spectroscopic studies on the darkening of lead white. *Appl. Spectrosc.* **2003**, *57*, 1393–1398. [[CrossRef](#)]
69. Monico, L.; Rosi, F.; Miliani, C.; Daveri, A.; Brunetti, B.G. Non-invasive identification of metal-oxalate complexes on polychrome artwork surfaces by reflection mid-infrared spectroscopy. *Spectrochim. Acta A Mol. Biomol. Spectrosc.* **2013**, *116*, 270–280. [[CrossRef](#)]
70. Mendes, N.; Lofrumento, C.; Migliori, A.; Castellucci, E.M. Micro-Raman and particle-induced X-ray emission spectroscopy for the study of pigments and degradation products present in 17th century coloured maps. *J. Raman Spectrosc.* **2008**, *39*, 289–294. [[CrossRef](#)]
71. Colombini, M.P.; Modugno, F.; Fuoco, R.; Tognazzi, A. A GC-MS study on the deterioration of lipidic paint binders. *Microchem. J.* **2002**, *73*, 175–185. [[CrossRef](#)]

Disclaimer/Publisher’s Note: The statements, opinions and data contained in all publications are solely those of the individual author(s) and contributor(s) and not of MDPI and/or the editor(s). MDPI and/or the editor(s) disclaim responsibility for any injury to people or property resulting from any ideas, methods, instructions or products referred to in the content.